# Strong signal increase in STED fluorescence microscopy by imaging regions of subdiffraction extent

Fabian Göttfert[a], Tino Pleiner[b], Jörn Heine[c], Volker Westphal[a], Dirk Görlich[b], Steffen J. Sahl[a], and Stefan W. Hell[a,1]

[a]Department of NanoBiophotonics, Max Planck Institute for Biophysical Chemistry, 37077 Göttingen, Germany; [b]Department of Cellular Logistics, Max Planck Institute for Biophysical Chemistry, 37077 Göttingen, Germany; and [c]Abberior Instruments GmbH, 37077 Göttingen, Germany

Contributed by Stefan W. Hell, January 11, 2017 (sent for review December 18, 2016; reviewed by Jörg Bewersdorf and Ke Xu)

**Photobleaching remains a limiting factor in superresolution fluorescence microscopy. This is particularly true for stimulated emission depletion (STED) and reversible saturable/switchable optical fluorescence transitions (RESOLFT) microscopy, where adjacent fluorescent molecules are distinguished by sequentially turning them off (or on) using a pattern of light formed as a doughnut or a standing wave. In sample regions where the pattern intensity reaches or exceeds a certain threshold, the molecules are essentially off (or on), whereas in areas where the intensity is lower, that is, around the intensity minima, the molecules remain in the initial state. Unfortunately, the creation of on/off state differences on subdiffraction scales requires the maxima of the intensity pattern to exceed the threshold intensity by a large factor that scales with the resolution. Hence, when recording an image by scanning the pattern across the sample, each molecule in the sample is repeatedly exposed to the maxima, which exacerbates bleaching. Here, we introduce MINFIELD, a strategy for fundamentally reducing bleaching in STED/RESOLFT nanoscopy through restricting the scanning to subdiffraction-sized regions. By safeguarding the molecules from the intensity of the maxima and exposing them only to the lower intensities (around the minima) needed for the off-switching (on-switching), MINFIELD largely avoids detrimental transitions to higher molecular states. A bleaching reduction by up to 100-fold is demonstrated. Recording nanobody-labeled nuclear pore complexes in *Xenopus laevis* cells showed that MINFIELD-STED microscopy resolved details separated by <25 nm where conventional scanning failed to acquire sufficient signal.**

fluorescence nanoscopy | STED microscopy | photobleaching | superresolution

Fluorescence nanoscopy or superresolution microscopy methods (1, 2) allow minimally invasive imaging with a resolution far beyond that of ordinary light microscopes. Recent advances open the possibility to resolve details at 20–50 nm and below (see examples in refs. 3–7). In stimulated emission depletion (STED) nanoscopy (8, 9)—as in all other fluorescence microscopy methods—the achievable resolution and contrast are largely determined by the total fluorescence signal, which is in turn limited by photobleaching. As a matter of fact, all superresolution concepts providing resolution at the 20- to 50-nm level are restricted to using specific fluorophores or buffers due to the signal limitation. Approaches previously developed to reduce photobleaching have therefore led to significant advances. Specifically, in STED nanoscopy, using long (>100-ps) laser pulses (10), reducing numbers of unnecessary state transition cycles (11), and allowing the relaxation of bleaching-prone dark fluorophore states (12) have already reduced photobleaching severalfold.

In STED microscopy (Fig. 1), resolution is increased by confining the capability of a fluorophore to emit fluorescence to a predefined subdiffraction-sized region. This is accomplished with the STED light, which forces excited fluorophores into their ground state through stimulated emission before fluorescence emission. Thus, the presence of STED light of a given intensity switches the fluorescence capability of the fluorophore off (Fig. 1*A*). To use this effect in a point-scanning microscope for superresolution, the focal-plane intensity distribution of a beam of STED light is typically formed to exhibit a central intensity zero ("doughnut"), switching off all fluorophores outside the vicinity of the focal center (Fig. 1 *B* and *C*). Both beams are jointly scanned through the specimen to successively probe neighboring subdiffraction sample regions where fluorophores may reside. We choose here to define the STED beam intensity $I_S$ as the intensity at which the probability of deexciting a fluorophore by stimulated emission is $p_{\text{stim}} = 0.5$. If the fluorophore is exposed to the intensity $I_S$, its fluorescence is reduced to 50% of its normal value (Fig. 1*A*).

We can now define $I_S$ as the threshold intensity that separates fluorophores that are "on" from those that are "off." In other words, if the fluorescence signal of a fluorophore is 50–100% of its normal signal, we define it as on; if it is <50%, we define it as off. Clearly, this definition is somewhat arbitrary, because we could also have chosen $6\,I_S$ as the threshold intensity, in which case off would have implied a signal reduction to only 1.56%. However, choosing $I_S$ has the advantage that it directly relates to the full width at half-maximum (FWHM) of the subdiffraction-sized region of fluorescence emission created by the doughnut-shaped STED beam, which is usually taken as a resolution measure. It is now important to realize that, although the fluorophores are off also for STED beam intensities that are higher than $I_S$, such higher intensities are actually not needed for keeping the fluorophore off, because the on/off difference is already created at $I_S$ (Fig. 1).

## Significance

**In stimulated emission depletion (STED) fluorescence microscopy, the diffraction resolution barrier is overcome by applying a doughnut-shaped light beam that transiently switches fluorescence off, confining molecular emission to subdiffraction-sized regions around the doughnut center. Unfortunately, the doughnut intensities required for high resolution exacerbate photobleaching. Our remedy, called MINFIELD, exploits the fact that fluorescence off-switching by STED does not require the high intensities of the doughnut crest. By recording subdiffraction-sized areas or volumes in the sample, molecular exposure to high intensities is avoided and photobleaching is reduced by more than 100-fold. Fluorescence analysis of cellular structures becomes possible in unprecedented detail. Providing larger signal and faster recording times, MINFIELD-STED microscopy should open a unique range of superresolution imaging applications in the life sciences.**

Author contributions: F.G., D.G., and S.W.H. designed research; S.W.H. conceived the MINFIELD approach; F.G. and J.H. performed research; T.P., V.W., and D.G. contributed new reagents/analytic tools; F.G. and J.H. analyzed data; and F.G., S.J.S., and S.W.H. wrote the paper.

Reviewers: J.B., Yale School of Medicine; and K.X., University of California, Berkeley.

Conflict of interest statement: S.W.H. and J.H. are a cofounder and employee of Abberior Instruments GmbH, respectively, a company commercializing superresolution microscopes. Jörg Bewersdorf and S.W.H. were coauthors on a paper in 2015: Hell SW, et al. (2015) The 2015 super-resolution microscopy roadmap. *J Phys D Appl Phys* 48(44):443001. This was a review article and not an active research collaboration.

Freely available online through the PNAS open access option.

[1]To whom correspondence should be addressed. Email: shell@gwdg.de.

This article contains supporting information online at www.pnas.org/lookup/suppl/doi:10.1073/pnas.1621495114/-/DCSupplemental.

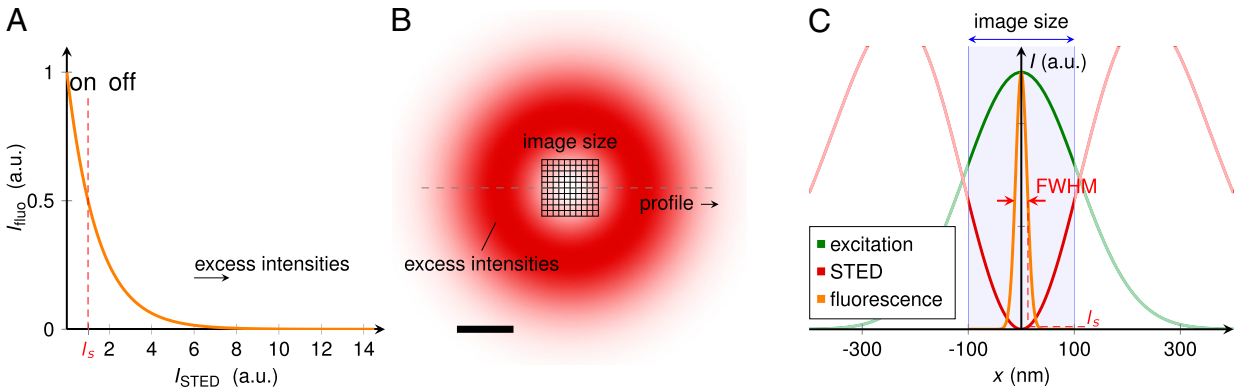


**Fig. 1.** The MINFIELD concept: Lower local deexcitation intensities in STED nanoscopy for image sizes below the diffraction limit. (*A*) In STED imaging with pulsed lasers, the ability of a fluorophore to emit fluorescence decreases nearly exponentially with the intensity of the beam deexciting the fluorophore by stimulated emission. We here define $I_s$ as the intensity at which the fluorescence signal is reduced by 50%. Fluorophores delivering higher signal are defined as on, whereas those with smaller signal are defined as off. (*B*) The STED beam is shaped to exhibit a central intensity zero in the focal region (i.e., a doughnut), so that (*C*) molecules can show fluorescence only if they are located in a small area in the doughnut center. This area decreases with increasing total doughnut intensity. Due to its diffraction-limited nature, the intensity distribution of the STED focal beam extends over more than half of the STED beam wavelength and exhibits strong intensity maxima, significantly contributing to bleaching. By reducing the size of the image field to an area below the diffraction limit, where the STED beam intensity is more moderate (i.e., around the doughnut minimum; compare image area indicated in *B*), one can reduce the irradiation intensities in the area of interest, inducing lower photobleaching and allowing the acquisition of more fluorescence signal at higher resolution. (Scale bar: 200 nm.)

However, intensities much greater than $I_S$ are applied in STED microscopy because tightly confining the region of possible fluorescence emission inevitably necessitates maxima (doughnut "crests") that are orders of magnitude stronger than what is required to switch the fluorophores off (Fig. 1*C*). Actually, these excess intensities only pay tribute to the fact that the doughnut profile is dictated by diffraction. Present over an area of several 100 nm in diameter, with maxima ~250 nm from the doughnut center, they do not define the on/off state contrast. However, they are the major cause for photobleaching at the periphery of the excitation spot.

The issue of these excess STED beam intensities has been recently addressed by driving fluorophores to an additional light-inert "protected" state in a concept termed "multiple off-state transitions" (MOST) nanoscopy (13). The rationale of MOST is that the process of fluorophore separation and hence resolution enhancement occurs in the immediate vicinity of the minimum (zero) of the state-separating switching light distribution. This long-standing insight (14), that information about the fluorophore(s) residing at the coordinate of the intensity minimum can be obtained right at the minimum by defining this coordinate with many photons, is also at the heart of the recently presented MINFLUX concept (15), enabling tracking and nanoscopy of fluorophores with minimal fluorescence fluxes.

Here, we demonstrate an approach leading to an improvement in total available fluorescence signal by two orders of magnitude on features <100 nm in size, by confining the imaged region almost to the spatial dimensions of the subdiffraction feature itself. Our approach maximizes the fluorescence signal attainable from the structure of interest, and enables imaging at higher resolution with higher signal-to-noise ratio (SNR). By reducing the image size (i.e., the field of view), the irradiation dose on the region of interest can be significantly reduced, as the strong light fields of the STED beam maxima (doughnut crests) are not scanned over the object to be imaged (Fig. 1 *B* and *C*). We have dubbed our approach MINFIELD because of two reasons. First, it reminds of the fact that our field of view is minimized to capture only the structure of interest and, second, it alludes to the fact that the molecules are exposed to those parts of the STED beam having minimal light fields. Depending on the image size and applied laser power, MINFIELD thus yields a strong reduction of photobleaching within the imaged region.

## Results

**Fast Addressing and Recording of Scanning Fields Below the Diffraction Limit.** The nanoscopy setup (*SI Materials and Methods*, Fig. S1, and Table S1) developed for our demonstration of the MINFIELD approach roughly followed the design considerations for red and far-red emitting dyes as reported previously (7). It used a 775-nm, 20-MHz pulsed STED laser, pulsed laser diodes at 595 and 635 nm for fluorescence excitation, and detection windows at 600–630 and 660–720 nm. However, scanning small areas poses additional challenges to the scanning system. Scaling down the typical scan parameters of a regular STED recording (10-nm pixel size, 100-µs pixel dwell time) to a total scan area of $100 \times 100$ nm$^2$ leads to a line frequency on the order of 1 kHz. As the whole imaged area is illuminated during the sequential acquisition of the pixels, photobleaching for subsequent positions increases. This can be avoided by repeatedly scanning the image at a timescale much shorter than the average fluorophore's survival time and summing the signal of consecutive image frames to acquire sufficient signal. The linearity of the scan process should be maintained despite the high imaging speed.

The focus positioning accuracy and repeatability of the beams must be better than 10 nm to allow nanometer-scale imaging. The accurate placement of the excitation and STED light foci at the desired scan position is especially challenging, because mechanical scanners can have a certain lag between the set and actual position due to their momentum. This lag may vary with the scan speed and scan position, and is typically several 100 nm. Approaching a target with an accuracy <50 nm, however, is crucial for the usability of the setup. These requirements are best satisfied by electro-optic scanners. They use the linear electro-optic effect to deflect the beam almost instantaneously when a voltage is applied, albeit by small angles. The scan range is therefore limited to a few micrometers. We used two electro-optic scanners for deflection in $x$ and $y$, allowing line frequencies above 100 kHz and reducing the positioning error to a negligible amount. To acquire larger overview images, a piezo stage with a scan range of 200 µm was used for scanning and positioning the sample in $x$, $y$, and $z$. Further details of the implementation can be found in *SI Materials and Methods*.

To select areas of interest for a STED scan, a large low-resolution image was first acquired with the piezo stage. The desired scan positions were then selected and approached with the piezo stage. A high degree of automation proved essential for productive imaging, as several imaging steps are required to reliably correct for sample drift or inaccurate positioning by the piezo stage. If required, several imaging iterations of decreasing size and increasing STED power could be combined to image the detailed structure on a small scale without losing the context on the large scale (Fig. S2). Dedicated imaging acquisition routines

were programmed with Python. As a future development, this iterative scanning with adaptive levels of STED resolution could be beneficially coupled with feature recognition and even machine-learning schemes that automate the selection of (biological) features of interest. Large datasets for hypothesis testing could thus be acquired with minimal input from the user.

**MINFIELD Imaging: Small Scan Fields Yield Major Signal Increases.** Fig. 2 demonstrates the potential of the altered scanning strategy on two-color STED images of immunolabeled nuclear pore complexes (NPCs). Although it is possible to image the whole nucleus in a single large scan, high laser intensities cause photobleaching; the same structures could not be imaged repeatedly (Fig. 2*A* and Fig. S3). In contrast, when the scan range was reduced to an area of 200 × 200 nm$^2$, more than 10 frames with sufficient signal were acquired (Fig. 2*B*), using otherwise unchanged imaging parameters (168-mW STED power, 100-μs pixel dwell time, 6.6-nm pixel size). It is thus possible to acquire an order of magnitude more signal from the structure than in a regular scan, opening up the way to image more complex samples with higher demand on resolution and SNR.

**Single-Fluorophore Assessments of Bleaching Reduction by MINFIELD.** To quantify the feasible improvements in signal yield under STED imaging conditions in more detail, we chose to investigate the photobleaching behavior of the dye Atto647N (Fig. 3 and Figs. S4 and S5). Atto647N is already established in STED imaging and has previously been used for bleaching experiments (4, 11, 16, 17). The bleaching dynamics of fluorescent dyes strongly depends on their molecular environment, including the dye density (18, 19) and oxygen concentration (20, 21). To achieve high reproducibility and control over the conditions in the sample, we prepared single-molecule samples of Atto647N-labeled double-stranded DNA (dsDNA) in PBS as described in refs. 16 and 22; the dye was attached at a 10-nm-long dsDNA strand with the opposing end immobilized on the coverslip. This configuration ensured free rotation of the dye molecule and removes it sufficiently from the influence of the coverslip surface.

For the experiment, fluorophores distributed at low density were individually identified in a confocal overview scan, their positions approached and the fluorescence signal measured for 20 s. As the survival time before photobleaching is on the order of a few seconds, most fluorophores bleach within this period. To ensure well-defined irradiation intensities, the vortex phase plate (VPP) (Fig. S1) responsible for the doughnut-shaped focus was removed from the beam path, and the excitation and only slightly larger STED foci were overlaid. To discriminate between reversible fluorescence preclusion and irreversible bleaching, the STED laser was blocked periodically with a chopper (30 Hz), while the fluorophore was illuminated with the excitation laser. The time $\tau$ until the molecule bleaches was derived from the data, and the bleaching rate calculated by averaging over ∼100 molecules: $r_{\text{combined}} = 1/\bar{\tau}$, with $\bar{\tau}$ denoting the average time until bleaching. The bleaching rate under STED conditions was calculated as follows:

$$r_{\text{STED}} = r_{\text{combined}} - r_{\text{probe only}},$$

where $r_{\text{probe only}}$ is the bleaching rate caused by the excitation beam alone. The photobleaching rate was observed to scale roughly linearly with the applied STED intensity (Fig. 3*A*). In separate measurements (Fig. S5*A*), the bleaching rate was found to depend linearly on the excitation intensity (3-μW average power for Fig. 3*A*) and to be comparatively low when the excitation laser was switched off completely. The excitation cross-section of the molecular ground state $S_0$ is negligibly low at the STED wavelength. A more detailed discussion of the bleaching behavior can be found in *SI Materials and Methods*, with additional data in Figs. S4 and S5.

A basic model intended to capture these observations considers (*i*) photobleaching from the $S_1$ state, and (*ii*) bleaching from higher states $S_n$ populated by further absorption of STED beam photons from $S_1$ (*SI Materials and Methods*). With this model, we simulated the bleaching behavior at various scan sizes (Fig. 3*B*)—now considering scanning with the STED doughnut configuration for nanoscopy—and compared the predictions to the experimental data. The bleaching probability of a single frame was calculated using the model by simulating the irradiation intensities at the image center for each pixel in the scan. The excitation laser focus was approximated with a Gaussian of 250 nm

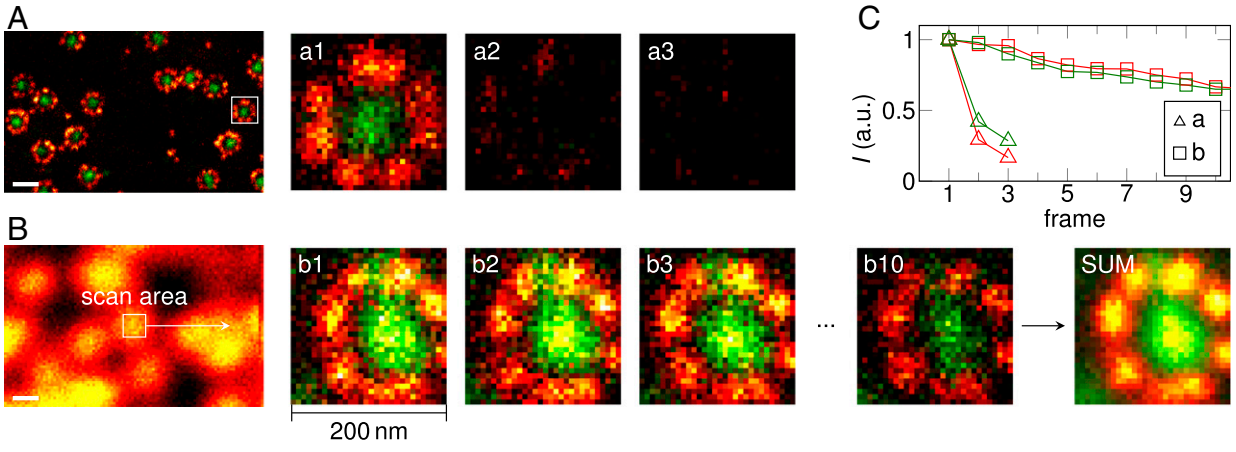


**Fig. 2.** Fluorescence signal increases when limiting the image field of STED nanoscopy to subdiffraction dimensions. The MINFIELD bleaching reduction is exemplified on amphibian nuclear pore complexes (NPCs) labeled with an anti-gp210 (red) and an anti-FG repeat Nup (green) antibody. (*A*) Details of the NPC structure are easily resolved in a conventional STED recording (full image in Fig. S3). However, due to photobleaching, acquiring several images was precluded in this case; the images *a1–a3* show the fluorescence signal of the highlighted area in subsequent recordings. (*B*) MINFIELD STED microscopy: reducing the scan area to the structure of interest increases the signal, as long as the area is smaller than the focal extent of the excitation and STED beams. To determine areas of interest, a low-resolution confocal image is acquired first. The selected area is then scanned multiple times (*b1–b10*) with high resolution. The signal can be summed up (SUM) or evaluated frame by frame. Color scale values (min, max) for this and all other image data are provided in Table S2, and the color scales are in Fig. S8. (*C*) Signals upon repeated imaging in the red and green channel of the images shown in *a1–a3* and *b1–b10*. (Scale bars: 200 nm.)

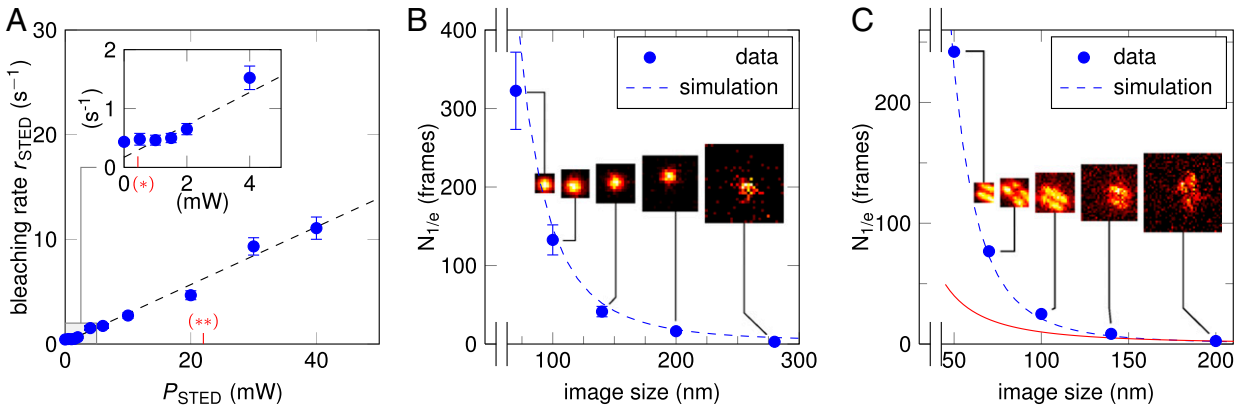


**Fig. 3.** Bleaching of the fluorophore Atto647N and the bleaching reduction brought about by MINFIELD recording. Bleaching was investigated by measuring single Atto647N molecules (in *A* and *B*) and Atto647N-labeled DNA-origami (in *C*). Dots represent experimental results, and lines are modeled according to Eq. S1 (*SI Materials and Methods*). Error bars indicate the derived SEM. (*A*) The bleaching rate $r_{STED}$ scales approximately linearly with the STED intensity, for constant excitation (3 μW). (*Inset* shows enlarged view of data for <5 mW.) The power levels indicated by (*) and (**) are associated with the $I_s$ and the doughnut crest intensity, respectively, used for the measurements in *B*. (*B* and *C*) Average number of frames $N_{1/e}$ before photobleaching of a single fluorophore (*B*) or DNA origami structure (*C*) vs. size of the scanned image field. (*B*) Decreasing the scan size of a STED measurement allows the acquisition of considerably more frames before the fluorophores bleach. (*C*) The increase in signal yield is readily observable also for more complex structures, such as labeled DNA origami. For comparison, the red curve shows a linear scaling with the inverse image area (normalized to the data point at 200 nm). It indicates the expected bleaching behavior if the average laser intensities in the imaged area were not to change with the image size (i.e., a bleaching reduction purely based on shorter exposure due to fewer-pixel scans). Here, a reduction from 200-nm image size to 50 nm (16-fold smaller area) allowed the acquisition of 100 times more frames.

FWHM, whereas the doughnut-shaped STED beam intensity was described by

$$I(d) = I_0 d^2 \exp\left(-\left(\frac{2d}{d_0}\right)^2\right),$$

where $I_0$ denotes the intensity scaling factor, $d$ is the distance from the center, and $d_0 = 468$ nm defines the peak-to-peak width of the STED doughnut.

The data points in Fig. 3*B* each represent the average number of frames $N_{1/e}$ before photobleaching of a single fluorophore. For each data point, ~100 molecules were measured. The STED average power was kept constant at 53 mW, and the pixel size was set to 10 nm. The *Insets* show representative images, with the signal of the first $N_{1/e}$ frames summed and the color scale scaled to the minimum and maximum pixel values (Table S2). Considerably more signal could be acquired when the scan range was reduced. Here, the difference between a scan range of 280 nm ($N_{1/e} = 3$) and 70 nm ($N_{1/e} = 320$) was more than 100-fold.

The model is readily applicable to other structures labeled with Atto647N, as exemplified on labeled DNA origami nanorulers (GATTA-STED 27R; GATTAquant), shown in Fig. 3*C*, basically consisting of two line-shaped fluorophore arrays arranged in parallel to each other at 27-nm distance. Although previously reported resolution values (3, 7) for STED microscopes would, in principle, have been sufficient to discern the two lines, our attempts failed in this case due to bleaching. The structure could be resolved, however, for a scan size of 200 nm. In this case, the signal was already reduced to less than a half after the first scan frame. To measure the 27-nm distance between the lines, a stronger signal was required, which was readily achieved by reducing the image size further. Providing absolute values for the improvement in signal yield is challenging, as fast photobleaching at large image sizes precludes accurate analysis. According to the model, a scan range of 200 nm would yield a fivefold increase in signal over that of a large scan, suggesting a 500-fold improvement at an image size of 50 nm. The origamis were imaged at a STED time-averaged power of 280 mW, 2.1-μW excitation power, 5-nm pixel size, and 100-μs pixel dwell time. The signal of ~100 single independently measured structures was summed up and the signal evolution with time in the image's central 2 × 2 pixels was fitted by an exponential decay with the bleaching constant $N_{1/e}$. The *Insets* of Fig. 3*C* show representative structures, with the signal summed over $N_{1/e}$ image frames and a normalized color scale. The dashed line describes the modeled bleaching behavior, scaled by a constant factor of 1.7. The need to slightly adjust the model to the experimental data are likely due to the different embedding media affecting the photobleaching.

**Enabling Nanoscale Imaging of Structures Labeled with Small Numbers of Fluorophores.** MINFIELD is especially relevant when using small camelid-derived single-domain antibodies (nanobodies) as labels. Although immunolabeling using primary and secondary antibodies gives high signal (>10 dyes per target), the resolution of STED nanoscopy already exceeds the size of the labeled antibody tree (Fig. 4*A*). Nanobodies are ~10-fold smaller than conventional antibodies and can therefore deliver fluorescent dyes very close to the actual target protein, offering an outstanding level of accuracy for superresolution microscopy (23, 24). However, because they can be tagged with only a few dyes, samples labeled via nanobodies provide lower signal, reducing the STED resolution attainable in practice. In Fig. 4 *B* and *C*, we demonstrate MINFIELD STED nanoscopy of nanobody-labeled NPCs resolving structures separated by as little as ~20 nm. Imaging with a larger scan size fails to acquire high-resolution images of sufficient quality (Fig. S6). The images show nuclear pores in *Xenopus laevis* X177 cells, labeled with recently developed nanobodies (23) against the nucleoporins Nup93 and Nup98. The laser powers were 252 mW for the STED and 2.1 μW for the excitation laser, the pixel size was set to 6.6 nm, and the cumulative pixel dwell time was 2 ms. The use of electro-optic scanners to image small areas reduces the need for extensive positioning correction by software and eliminates the overhead of turning points required to accelerate mechanical scanners. Although useful, electro-optic scanning is not critical for the implementation of MINFIELD, as shown in the next demonstration.

**MINFIELD Is Especially Beneficial for STED Imaging Along the Optic Axis.** Fig. 5 demonstrates the MINFIELD approach in 3D, on a STED system using galvanometer scanners for image acquisition (Abberior Instruments; QUAD Scan superresolution microscope, modified with a home-built pulsed STED laser, operating at 40 MHz and 775 nm). Here, the laser light is turned off by acousto-optical modulators during the turning points of the scan mirrors. For the STED beam, a partial beam passing a 2π phase vortex and another one passing a top-hat phase pattern are

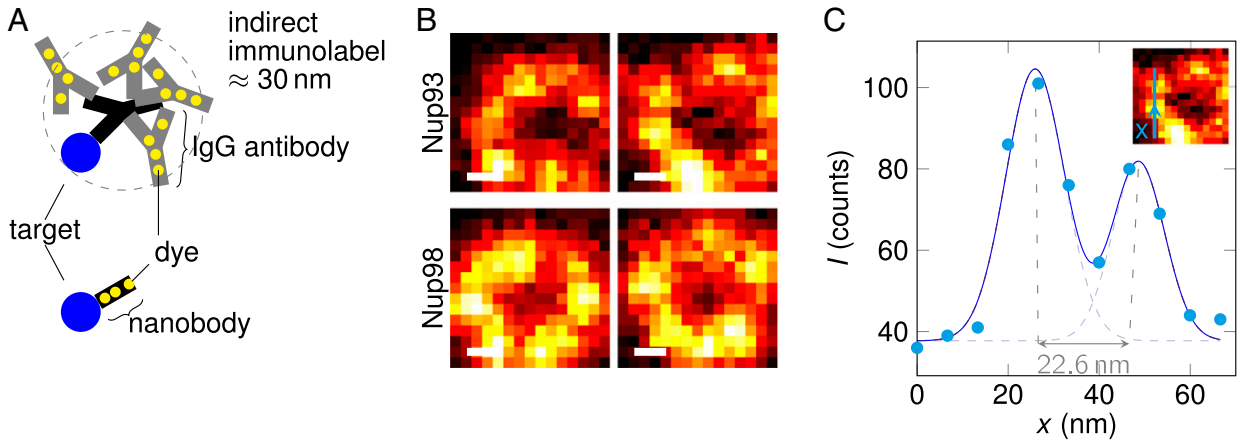


**Fig. 4.** MINFIELD STED nanoscopy of samples with low fluorophore-to-protein ratio. Here, Abberior Star Red-labeled nanobodies are used to visualize the arrangement of Nup93 and Nup98 within the amphibian NPC. Nup93 forms a ring around the center of the nuclear pore with a diameter of ∼70 nm. Its substructure (*A*) would be obscured by the size of the antibody tree in conventional indirect immunolabeling. Using nanobodies reduces the number of dye molecules per protein considerably. (*B*) Limiting the scan field compensates this effect and images detailed cellular structures with high SNR at ∼20-nm resolution. *C* shows a line profile through the Nup93 image at the indicated position. The data were fitted with two Gaussians, yielding a peak-to-peak separation smaller than 23 nm and a full width at half-maximum of ∼15 nm for the individual Gaussians. (Scale bars: 20 nm.)

overlaid incoherently. The relative powers are chosen for the focal STED light intensity distribution to yield approximately isotropic resolution increase in 3D (Fig. 5*A*). Compared to a configuration with similar 2D (lateral) resolution improvement, the laser intensities are much larger and spread over a wider area, indicating that in 3D STED microscopy confining the scanned region is especially advantageous.

Fig. 5*B* demonstrates the resolution improvement of STED compared with conventional confocal microscopy on Atto647N-labeled DNA origami (GattaQuant; custom structure according to ref. 25), with a line profile analysis revealing the resolution increase along *z* (Fig. 5*C*). The total STED power of 294 mW was split between the phase patterns, with 10% used for the vortex phase pattern and 90% for the top-hat pattern. The pixel dwell time was set to 10 µs (STED) and 1 µs (conf), with a pixel size of 10 nm. Ten frames were summed for display in Fig. 5*B*. Fig. 5*D* demonstrates the bleaching reduction per acquired frame using the pure top-hat pattern with a constant scan range of 5 µm in the *x* direction. The data were acquired by repeatedly imaging immunolabeled microtubules of Vero cells with a STED average power of 168 mW, yielding a resolution of ∼80 nm in *z*. Confining the scan range in *z* to 200 nm readily reduced the bleaching per frame 10-fold.

## Discussion and Conclusions

We have shown that STED nanoscopy can yield over 100 times more signal than usual when the imaged region is limited to a size well below the diffraction limit. The potential of our MINFIELD approach was demonstrated on different sample types, from single molecules to complex structures such as NPCs. We investigated the bleaching behavior of Atto647N in single-molecule experiments and found a linear relationship between the bleaching rate and the light intensities for the studied regime. These results agree well with published data (17) and can be used to estimate the bleaching rate in STED measurements. It should be noted, however, that the bleaching behavior strongly depends on

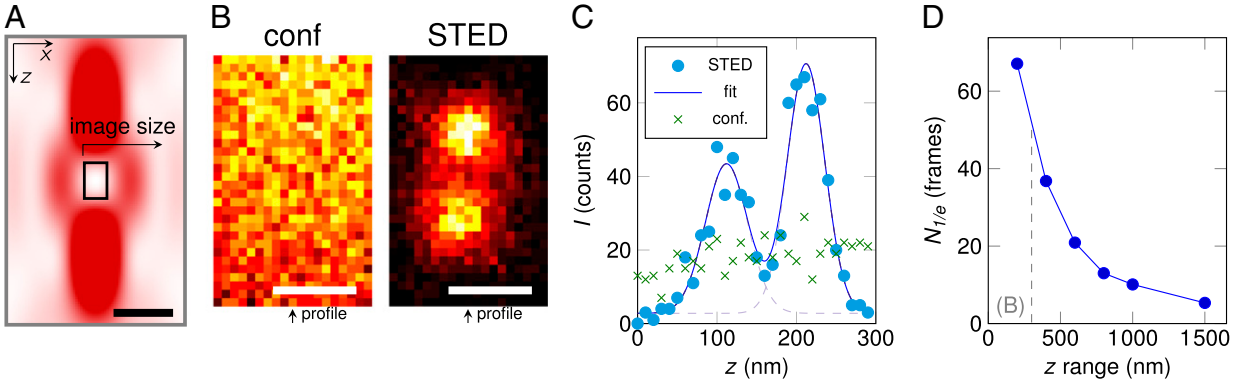


**Fig. 5.** MINFIELD is especially advantageous for STED imaging along the optic axis (*z*) and in 3D. (*A*) The focal STED intensity distribution for confining molecular fluorescence along the optic axis (*z*) and hence in 3D extends well over >1 µm in *z*. Achieving similar resolution as in the focal plane requires higher laser intensities. (*B*) Three-dimensional imaging is demonstrated on Atto647N-labeled DNA origami with two spots designed to be separated by 91 nm. The resolution improvement with STED is immediately apparent when comparing the confocal *xz* image with its MINFIELD STED counterpart. (*C*) Analyzing the line profile along the *z* axis yields a peak-to-peak separation of ∼100 nm at a full width at half-maximum of ∼60 nm for the Gaussian fits. (*D*) Number of image frames that could be acquired before the fluorescence signal dropped below 1/*e* of its original brightness, depending on the scan range along the *z* axis. The data were acquired by imaging antibody-labeled microtubules in an *x*–*z* scan, using a "top-hat"–only phase pattern and keeping the *x*-range constant at 5 µm (see data in Fig. 3 *B* and *C*, where the imaged fields were squares, and, consequently, the relative area reductions stronger than for the data shown here). The indicated *z* range (dashed line) corresponds to the size of the images in *B*. [Scale bars: 500 nm (*A*), 100 nm (*B*).]

the dye used and on the sample type. Dyes other than Atto647N may be more prone to bleaching by the STED laser alone, which would even increase the benefit of the MINFIELD strategy. At present, our approach appears important for STED imaging of samples labeled with organic fluorophores at a low dye-per-protein ratio, such as nanobodies or SNAP tags. In these cases, plain STED nanoscopy scanning of a large field of view cannot acquire sufficient signal at high resolution, yet the reduction of image size should reveal details separated by only 20 nm with sufficient contrast levels. The increase in signal yield will also be beneficial to applications requiring high photon counts, such as the counting of molecules (22).

Furthermore, a simple estimation (*SI Materials and Methods* and Fig. S7) shows that the minimal number of pixels per dimension fulfilling the Nyquist sampling condition is given by the square root of the ratio of the highest intensity allowed within the imaging range divided by $I_S$. Note that neither the wavelength nor the maximum intensity of the (doughnut- or standing-wave–shaped) STED light affect this number. Obviously, the resolution and the maximum field of view are tightly connected. Intensity-induced limitations can be avoided if the ratio of the image size (edge length) to the resolution is kept constant. It should also be noted that in MINFIELD scanning the exposure of the fluorophores to (high) intensities varies across the field of view, with the field of view center experiencing the lowest intensities on average.

A fundamental concept, MINFIELD will also be applicable to other types of coordinate-targeted superresolution variants, such as ground-state depletion (26) and reversible saturable/switchable optical fluorescence transitions (RESOLFT) nanoscopy using photoswitchable fluorescent proteins (27–29) and switchable (photochromic) synthetic-organic fluorophores (30). Moreover, MINFIELD will be relevant for superresolution modalities that use light patterns for switching fluorophores on rather than off. This applies not only to the methods that saturate the activation of fluorescent proteins using a pattern of light (31, 32), but also to those that rely on depleting the ground state by pumping the fluorophore to a higher-lying state, in particular the fluorescent state, as is the case in so-called saturated structured illumination microscopy (33, 34), which is substantially more prone to photobleaching than STED microscopy. For all of these ground-state depletion-type approaches (26, 32–34), confining the imaging to subdiffraction-sized regions (around the intensity minimum) should be beneficial. Last but not least, our MINFIELD strategy can be combined with other approaches to reduce photobleaching, such as optimizing the sample buffer (4), dark-state relaxation (12), and reducing the number of state transition cycles (11). Confining the image size to an area below the diffraction limit will extend the capabilities of superresolved fluorescence analysis toward applications where high signal-to-noise and superior resolution are of essential importance.

## Materials and Methods

Detailed descriptions of the optical setup, image acquisition, and sample preparation including nanobody labeling, as well as single-molecule bleaching measurements and a calculation of the number of useful pixels, are provided in *SI Materials and Methods*. In brief, MINFIELD nanoscopy was demonstrated with a custom-built point-scanning dual-color STED setup (7) adapted to incorporate electro-optic rapid scanning of subdiffraction-sized image fields. Piezo scanning was used to image large areas of the sample and to center areas of interest for small-area scans. The minimum at the center of a doughnut-shaped focal intensity distribution for fluorescence deexcitation was formed as previously by imprinting a $2\pi$ vortex phase pattern on the STED beam's wave front with a dedicated phase plate.

**ACKNOWLEDGMENTS.** We thank Dr. H. Ta for help with the single-molecule and origami samples, Dr. V. Cordes for providing antibodies, Dr. V. Belov for providing KK114-maleimide in early nanobody labeling experiments, and T. Gilat and Dr. E. Rothermel (all Max Planck Institute for Biophysical Chemistry) for technical assistance. Dr. M. Reuss (Abberior Instruments GmbH) is acknowledged for support and help with the experiments on the galvanometer scanning system. S.W.H. acknowledges funding by the Göttingen Excellence Center for Nanoscale Microscopy and Molecular Physiology of the Brain.

1. Hell SW (2007) Far-field optical nanoscopy. *Science* 316(5828):1153–1158.
2. Huang B, Babcock H, Zhuang X (2010) Breaking the diffraction barrier: Super-resolution imaging of cells. *Cell* 143(7):1047–1058.
3. Donnert G, et al. (2006) Macromolecular-scale resolution in biological fluorescence microscopy. *Proc Natl Acad Sci USA* 103(31):11440–11445.
4. Kasper R, et al. (2010) Single-molecule STED microscopy with photostable organic fluorophores. *Small* 6(13):1379–1384.
5. Shtengel G, et al. (2009) Interferometric fluorescent super-resolution microscopy resolves 3D cellular ultrastructure. *Proc Natl Acad Sci USA* 106(9):3125–3130.
6. Aquino D, et al. (2011) Two-color nanoscopy of three-dimensional volumes by 4Pi detection of stochastically switched fluorophores. *Nat Methods* 8(4):353–359.
7. Göttfert F, et al. (2013) Coaligned dual-channel STED nanoscopy and molecular diffusion analysis at 20 nm resolution. *Biophys J* 105(1):L01–L03.
8. Hell SW, Wichmann J (1994) Breaking the diffraction resolution limit by stimulated emission: Stimulated-emission-depletion fluorescence microscopy. *Opt Lett* 19(11):780–782.
9. Klar TA, Jakobs S, Dyba M, Egner A, Hell SW (2000) Fluorescence microscopy with diffraction resolution barrier broken by stimulated emission. *Proc Natl Acad Sci USA* 97(15):8206–8210.
10. Dyba M, Hell SW (2003) Photostability of a fluorescent marker under pulsed excited-state depletion through stimulated emission. *Appl Opt* 42(25):5123–5129.
11. Staudt T, et al. (2011) Far-field optical nanoscopy with reduced number of state transition cycles. *Opt Express* 19(6):5644–5657.
12. Donnert G, Eggeling C, Hell SW (2007) Major signal increase in fluorescence microscopy through dark-state relaxation. *Nat Methods* 4(1):81–86.
13. Danzl JG, et al. (2016) Coordinate-targeted fluorescence nanoscopy with multiple off states. *Nat Photonics* 10(2):122–128.
14. Hell SW (2015) Nanoscopy with focused light (Nobel Lecture). *Angew Chem Int Ed Engl* 54(28):8054–8066.
15. Balzarotti F, et al. (December 22, 2016) Nanometer resolution imaging and tracking of fluorescent molecules with minimal photon fluxes. *Science*, 10.1126/science.aak9913.
16. Vogelsang J, et al. (2008) A reducing and oxidizing system minimizes photobleaching and blinking of fluorescent dyes. *Angew Chem Int Ed Engl* 47(29):5465–5469.
17. Wu Y, et al. (2015) Resonant scanning with large field of view reduces photobleaching and enhances fluorescence yield in STED microscopy. *Sci Rep* 5:14766.
18. Chen RF, Knutson JR (1988) Mechanism of fluorescence concentration quenching of carboxyfluorescein in liposomes: Energy transfer to nonfluorescent dimers. *Anal Biochem* 172(1):61–77.
19. Luchowski R, et al. (2008) Single molecule studies of multiple-fluorophore labeled antibodies. Effect of homo-FRET on the number of photons available before photobleaching. *Curr Pharm Biotechnol* 9(5):411–420.
20. Zondervan R, Kulzer F, Kol'chenk MA, Orrit M (2004) Photobleaching of rhodamine 6G in poly (vinyl alcohol) at the ensemble and single-molecule levels. *J Phys Chem A* 108(10):1657–1665.
21. Song L, Hennink EJ, Young IT, Tanke HJ (1995) Photobleaching kinetics of fluorescein in quantitative fluorescence microscopy. *Biophys J* 68(6):2588–2600.
22. Ta H, et al. (2015) Mapping molecules in scanning far-field fluorescence nanoscopy. *Nat Commun* 6:7977.
23. Pleiner T, et al. (2015) Nanobodies: Site-specific labeling for super-resolution imaging, rapid epitope-mapping and native protein complex isolation. *eLife* 4:e11349.
24. Ries J, Kaplan C, Platonova E, Eghlidi H, Ewers H (2012) A simple, versatile method for GFP-based super-resolution microscopy via nanobodies. *Nat Methods* 9(6):582–584.
25. Schmied JJ, et al. (2013) DNA origami nanopillars as standards for three-dimensional superresolution microscopy. *Nano Lett* 13(2):781–785.
26. Hell SW, Kroug M (1995) Ground-state depletion fluorescence microscopy, a concept for breaking the diffraction resolution limit. *Appl Phys B* 60(5):495–497.
27. Hell SW (2003) Toward fluorescence nanoscopy. *Nat Biotechnol* 21(11):1347–1355.
28. Hofmann M, Eggeling C, Jakobs S, Hell SW (2005) Breaking the diffraction barrier in fluorescence microscopy at low light intensities by using reversibly photoswitchable proteins. *Proc Natl Acad Sci USA* 102(49):17565–17569.
29. Grotjohann T, et al. (2011) Diffraction-unlimited all-optical imaging and writing with a photochromic GFP. *Nature* 478(7368):204–208.
30. Roubinet B, et al. (2016) Carboxylated photoswitchable diarylethenes for biolabeling and super-resolution RESOLFT microscopy. *Angew Chem Int Ed Engl* 55(49):15429–15433.
31. Rego EH, et al. (2012) Nonlinear structured-illumination microscopy with a photoswitchable protein reveals cellular structures at 50-nm resolution. *Proc Natl Acad Sci USA* 109(3):E135–E143.
32. Li D, et al. (2015) Extended-resolution structured illumination imaging of endocytic and cytoskeletal dynamics. *Science* 349(6251):aab3500.
33. Heintzmann R, Jovin TM, Cremer C (2002) Saturated patterned excitation microscopy—a concept for optical resolution improvement. *J Opt Soc Am A Opt Image Sci Vis* 19(8):1599–1609.
34. Gustafsson MGL (2005) Nonlinear structured-illumination microscopy: Wide-field fluorescence imaging with theoretically unlimited resolution. *Proc Natl Acad Sci USA* 102(37):13081–13086.
35. Wurm CA, Neumann D, Schmidt R, Egner A, Jakobs S (2010) Sample preparation for STED microscopy. *Methods Mol Biol* 591:185–199.
36. Cordes VC, Gajewski A, Stumpp S, Krohne G (1995) Immunocytochemistry of annulate lamellae: Potential cell biological markers for studies of cell differentiation and pathology. *Differentiation* 58(4):307–312.
37. Eggeling C, Volkmer A, Seidel CAM (2005) Molecular photobleaching kinetics of Rhodamine 6G by one- and two-photon induced confocal fluorescence microscopy. *ChemPhysChem* 6(5):791–804.
38. Kasha M (1950) Characterization of electronic transitions in complex molecules. *Discuss Faraday Soc* 9:14–19.